[Patrice Abry, Stéphane G. Roux, Herwig Wendt, Paul Messier, Andrew G. Klein, Nicolas Tremblay, Pierre Borgnat, Stéphane Jaffard, Béatrice Vedel, Jim Coddington, and Lee Ann Daffner]

Multiscale Anisotropic Texture Analysis and Classification of Photographic Prints

© GHENT, KATHEDRALE KERKFABRIEK: PHOTO COURTESY OF KIK-IRPA, BRUSSELS. MAGNIFYING GLASS—IMAGE LICENSED BY INGRAM PUBLISHING.
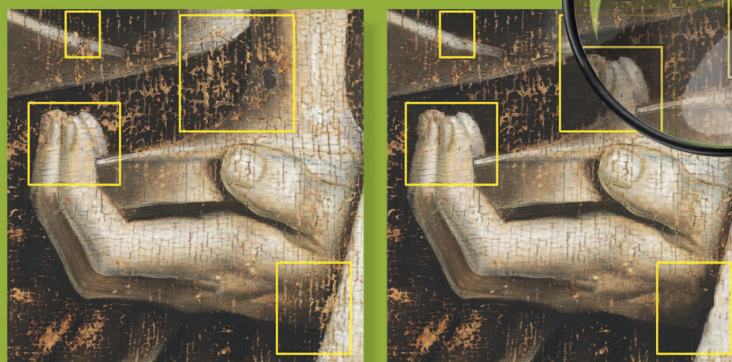
Signal Processing for Art Investigation

[Art scholarship meets image processing algorithms]

Texture characterization of photographic prints can provide scholars with valuable information regarding photographers' aesthetic intentions and working practices. Currently, texture assessment is strictly based on the visual acuity of a range of scholars associated with collecting institutions, such as museum curators and conservators. Natural interindividual discrepancies, intraindividual variability, and the large size of collections present a pressing need for computerized and automated solutions for the texture characterization and classification of photographic prints. In the this article, this challenging image processing task is addressed using an anisotropic multiscale representation of texture, the hyperbolic wavelet transform (HWT), from which robust multiscale features are constructed. Cepstral distances aimed at ensuring balanced multiscale contributions are computed between pairs of images. The resulting large-size affinity matrix is then clustered

using spectral clustering, followed by a Ward linkage procedure. For proof of concept, these procedures are first applied to a reference data set of historic photographic papers that combine several levels of similarity and second to a large data set of culturally valuable photographic prints held by the Museum of Modern Art in New York. The characterization and clustering results are interpreted in collaboration with art scholars with an aim toward developing new modes of art historical research and humanities-based collaboration.

INTRODUCTION

Surface texture is a defining characteristic of a photographic print and has a significant impact on the quality and perception of the image. Manufacturers of both traditional photographic paper and new-generation inkjet materials thus carefully engineer surfaces to meet a variety of functional and expressive requirements. Smoother surfaces typically produce images with greater optical saturation and tonal range. With good lighting, smooth, featureless surfaces can visually negate the picture plane. Reducing this perceptual barrier can transform a two-dimensional (2-D) image into a more effective illusion of objective reality. Rougher surfaces cause more scattering of incident light providing the viewer with a greater tactile sense of the print as a material object. A stronger physical presence can often convey heightened intrinsic value and expressive weight. Understanding how these qualities are manipulated provides scholars insight into artistic intent and practice. More practically, as an indelible physical attribute, print texture can help categorize preferred and anomalous papers within an artist's body of work or identify anomalies (including fakes). Encyclopedic reference collections of such textures, cataloged by manufacturer and date, are currently being assembled for both traditional [1] and inkjet [2] photographic materials. Likewise, the very beginning steps are underway to catalog surface textures used by prominent photographers such as Man Ray and Lewis Hine, among others [3]. While presently useful, such surface texture collections are difficult to catalog and access, as tools for query and retrieval are only in early stages of development. At present, experts visually and manually classify an unknown texture by comparing it with identified references. This is a tedious and challenging task due to the sheer size of available reference collections exposing a significant need for (semi)automated procedures to assist in texture assessment.

Texture analysis and characterization are long-standing topics of image processing and have been the subject of considerable research efforts over the past decades, cf., e.g., [4]–[8]. Texture characterization has relied on a variety of attributes
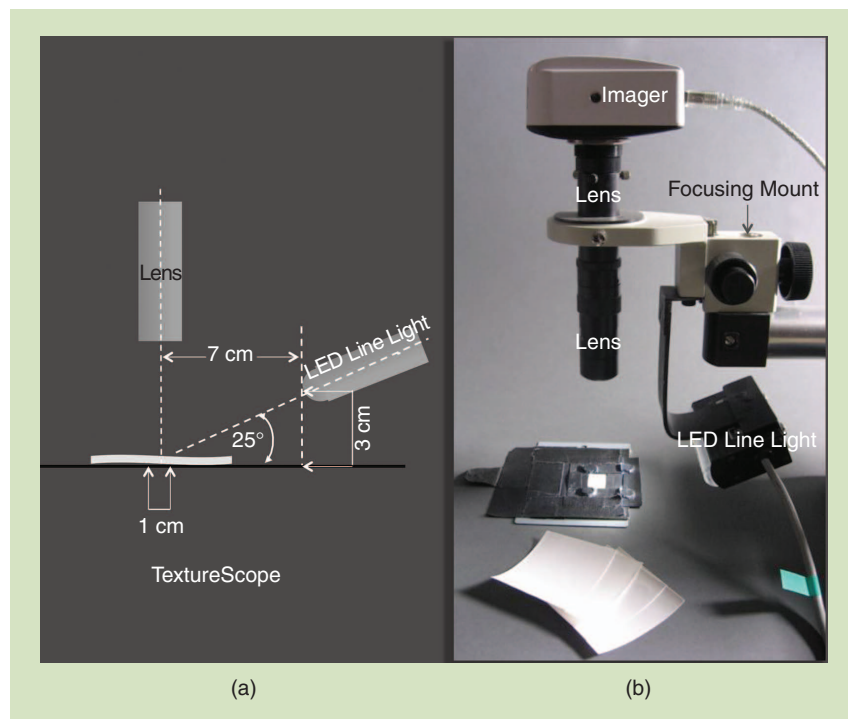
[FIG1] The TextureScope.

(from textons or primitives, i.e., gray-level statistics or geometrical features, to co-occurrence matrices or multiple spatial dependencies) and has proven effective for a wide range of different applications, e.g., in biomedical contexts [9], [10], in physics of surfaces and fractures [11], and in geophysics [12]. To a lesser extent, and only recently, texture analysis has been applied to art investigations (cf. [13]–[22] and the references therein). Among the many paradigms used for texture characterization, fractal and multiscale methods have received growing attention. Fractal analysis has further been extended to multidimensional multifractal analysis, cf., e.g., [17] and [23]. However, in most formulations, (multi)fractal or multiscale analyses do not account for the potential anisotropy of textures. Recently, however, the HWT [24] has been shown to account for anisotropy in the multiscale analysis of textures [25].

DATA SETS

TEXTURE IMAGE ACQUISITION

Presently, the simplest means to catalog surface texture is through images made using magnification and raking light. This imaging system, referred to as the *TextureScope*, has been extensively described in [19] and is shown in Figure 1. It is noncontact and nondestructive and can therefore be easily adapted for use on photographic prints of high intrinsic value. The method is relatively quick and requires minimal specialized handling so that large image sets can be produced rapidly. Created under repeatable and standardized conditions, the resulting images provide an important visual record and serve as a basis for computational analysis. The TextureScope depicts 1.00×1.35 cm^2 of a paper

surface. This scale is selected since it reveals some microscopic features, such as matting agents occasionally used by manufacturers, but also depicts attributes recognizable to a human observer. Samples are digitized at 153.6 pixel/mm, resulting in $1{,}536 \times 2{,}080$ images, with each pixel thus corresponding to $6.51^2 \simeq 42.4\,\mu m^2$.
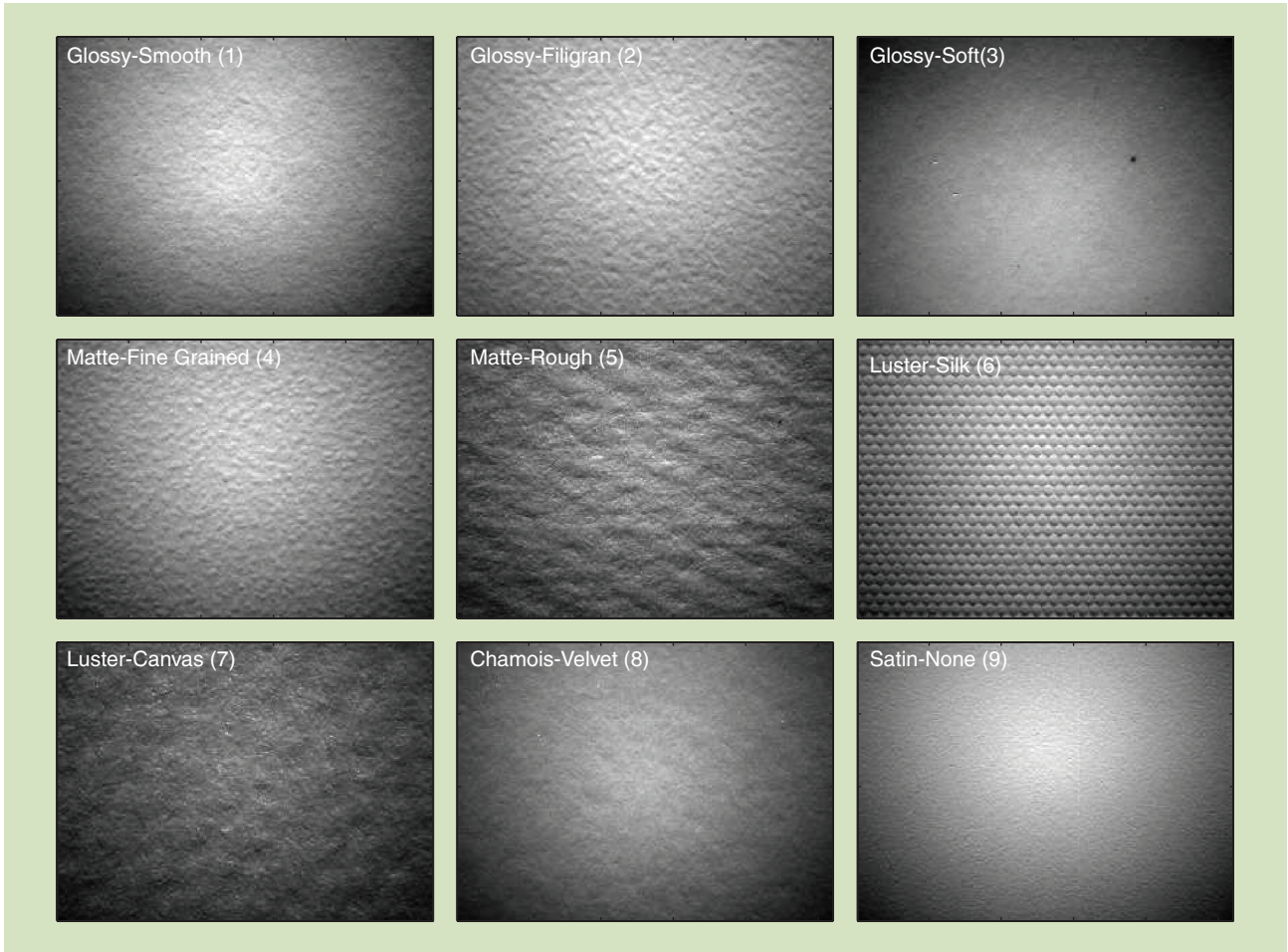
PHOTOGRAPHIC PAPER TEXTURE DATA SETS

Data set 1 consists of 120 nonprinted photographic paper samples. Aside from the texture images, the data set includes manufacturer-applied semantic descriptions of the samples (manufacturer, brand, texture, and reflectance) and an approximate date of production. Three levels of similarity are built into the data set (cf. Figure 2): 1) samples from one same sheet (three subsets of ten samples each), 2) samples from sheets taken from one same package (three subsets of ten samples each), and 3) samples from papers made to the same manufacturer specifications over a period of time (three subsets of ten samples each). In addition, 30 sheets representing a fuller diversity of photographic paper textures are included. The data set and its documentation have been prepared by an expert familiar with the technical and aesthetic history of photographic paper to include both commonly used surfaces and some outliers. Data set 1, further described in [19], is publicly available within the framework of the Historic Photographic Paper Classification Challenge (http://papertextureid.org) developed by Paul Messier and C.R. Johnson.

Data set 2 gathers 2,491 samples that fall into two subset categories. The first and largest subset (2,031 samples) consists of silver gelatin (traditional black and white paper) surface texture samples that were taken directly from manufacturer packages or sample books spanning the 20th century. These samples are representative of the full range of surface textures available to 20th century photographers and is carefully documented using the same manufacturer-applied metadata described for data set 1. The second subset in data set 2 contains textures from finished photographic prints. Within this group, 346 samples derive from the Thomas Walther collection held by the Museum of Modern Art in New York and contains work by leading modernist photographers primarily active in Central and Eastern Europe between World War I and World War II. This group is joined by a small but important collection of textures from 11 prints belonging to the Museum of Fine Arts, Houston. Each one of the 11 prints are by the same artist and depict the same image as 11 prints from the Walther collection in the Museum of Modern Art. Comparing the textures of these twin prints offers the possibility of determining if they are made on exactly the same, similar, or completely different papers. Discovering a shared material history between the print pairs can have significant ramifications for art historical
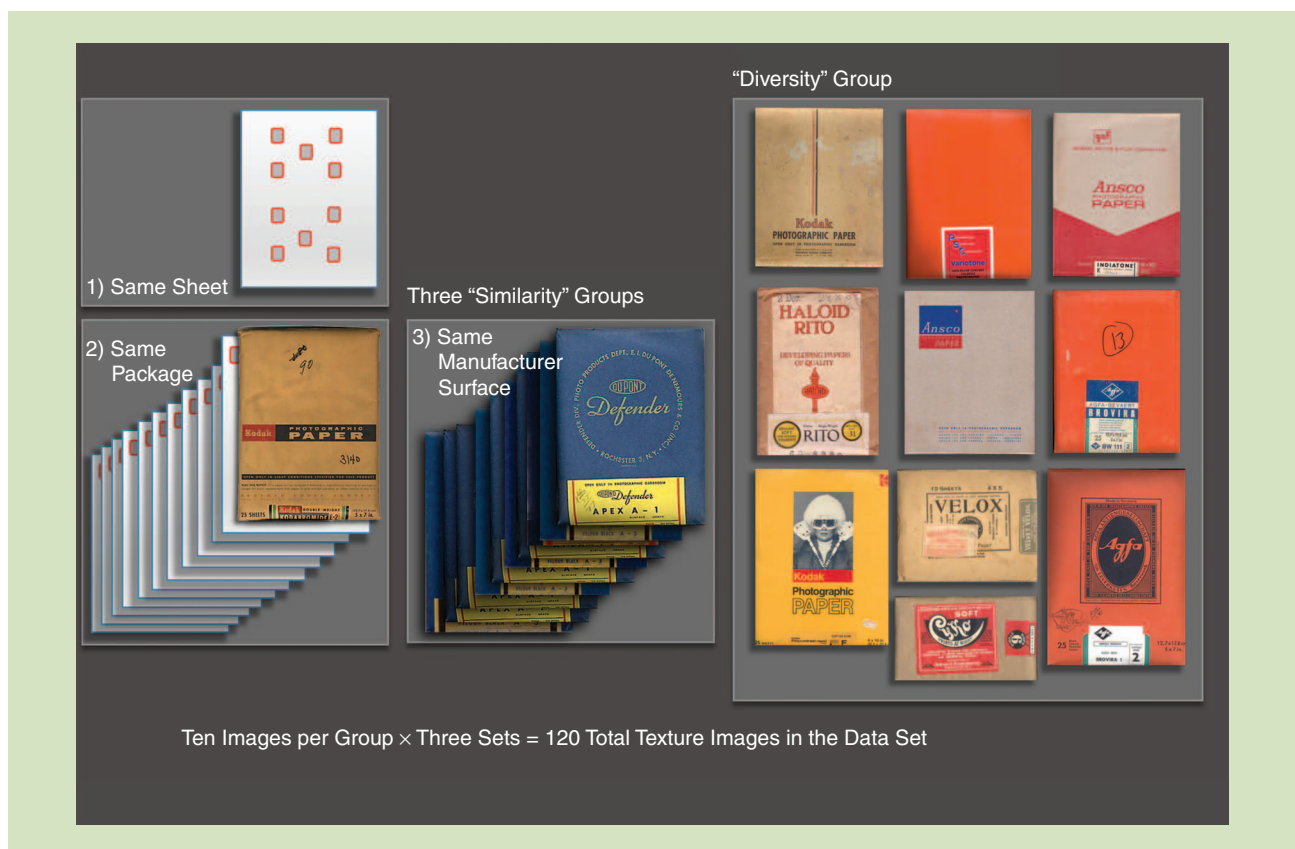
[FIG2] Data set 1 with nine groups of ten samples, each representing three levels of similarity (same sheet, same packet, same manufacturer) and 30 samples representing the diversity of art photographic papers.

[FIG3] Photographic paper textures. Examples of raking light photographic paper samples spanning a variety of different reflectance-texture characteristics.

scholarship, especially if this link can be established remotely through data analysis versus often impractical side-by-side comparison. Data set 2 thus offers rich opportunities for cross-referencing discovered affinities and anomalies across time periods, manufacturers, collections, and individual makers. Typical samples from data set 2 are represented in Figure 3, spanning a variety of photographic papers.

METHODOLOGY

A texture-clustering procedure relies on the selection, design, and combination of three key ingredients: 1) features representative of the texture, 2) the distances between features providing relevant measurement of resemblance between pairs of paper surfaces, and 3) the classification procedure.

FEATURES: HYPERBOLIC WAVELET TRANSFORM

We propose to extract surface features using the HWT [24]. HWT consists of one of the many variations in image multiscale analysis, that expands on the classical 2-D-discrete wavelet transform (2-D-DWT). HWT explicitly accounts for the potential anisotropy of an image texture, as it relies on the use of two independent dilation factors $a_1 = 2^{j_1}$ and $a_2 = 2^{j_2}$
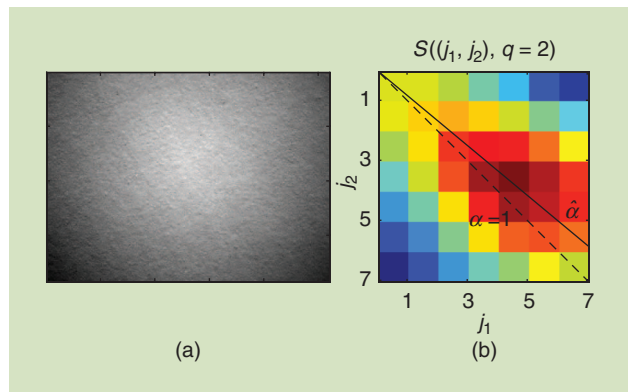

[FIG4] HWT-based features. (a) A surface sample with its (b) HWT-based anisotropic multiscale representation $S_X(j_1, j_2, q = 2)$. The estimated anisotropy angle $\hat{\alpha}_{0,q=2}$ (solid line) indicates a departure from isotropy $\alpha \equiv 1$ (dashed line).

along the horizontal and vertical axes. In [25], HWT is favorably compared against the 2-D-DWT, the former permitting to disentangle actual multiscale properties from the potential anisotropy of the analyzed texture, while the latter yields
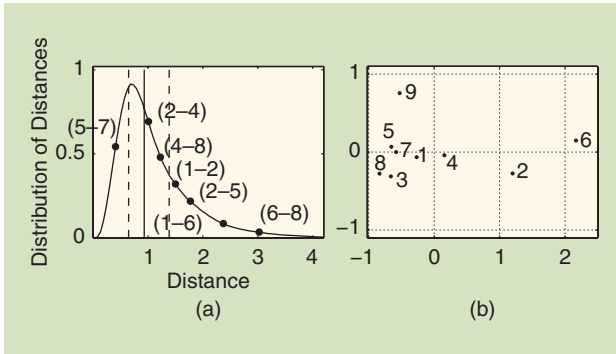
[FIG5] The distances between (a) photographic paper textures between all pairs of data set 2, to which are reported distances between some of the samples shown in Figure 3(a), and (b) a virtual 2-D space showing proximity between samples (see the "Methodology" section for more details).
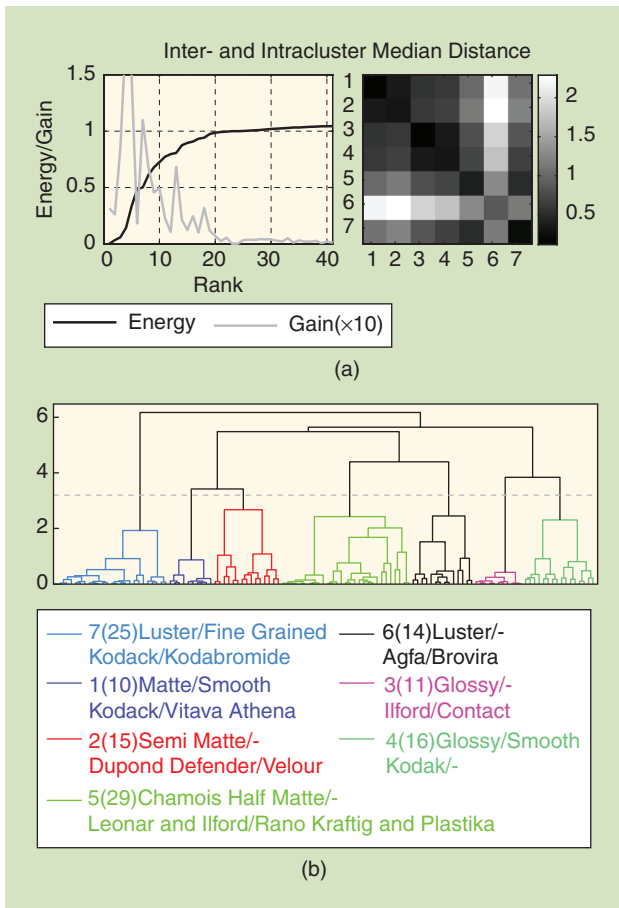
[FIG6] Data set 1: spectral clustering. The left plot in (a) shows the sorted eigenvalues (energy) and successive differences (gain), while the right plot shows the intra- and intercluster median distances. (b) A dendrogram showing seven clusters, with a posteriori interpretations of their contents from the manufacturer-applied metadata: cluster # (cluster size): reflectance/texture, manufacturer/brand.

strongly biased estimates of multiscale properties when textures are anisotropic.

The HWT coefficients of an image $X(x_1, x_2)$ are obtained by comparing it, by means of inner product, against a collection of dilated [at scales $\mathbf{a} = (2^{j_1}, 2^{j_2})$] and translated [at locations $(2^{j_1}k_1, 2^{j_2}k_2)$] templates

$$\psi_{j_1,j_2,k_1,k_2}(x_1,x_2) = 2^{-(j_1+j_2)/2}\psi_0(2^{-j_1}x_1 - k_1, 2^{-j_2}x_2 - k_2) \quad (1)$$

of a reference mother-wavelet $\psi_0(x_1, x_2)$, $\forall (j_1, j_2) \in \mathbb{R}_+^2$:

$$T_X(j_1, j_2, k_1, k_2) = \langle X(x_1, x_2), \psi_{j_1,j_2,k_1,k_2}(x_1, x_2) \rangle. \quad (2)$$

The mother-wavelet $\psi_0(x_1, x_2)$ is classically defined as a tensor-product of one-dimensional (1-D)-multiresolution mother-wavelets (cf., e.g., [28]). A multiscale representation of $X(x_1, x_2)$ is further obtained by computing space averages (l^q-norms) of the $T_X(j_1, j_2, k_1, k_2)$ at fixed scale pairs (j_1, j_2), $q > 0$:

$$S_X(j_1, j_2, q) = \frac{1}{n_a}\sum_{k_1, k_2} |T_X(j_1, j_2, k_1, k_2)|^q, \quad (3)$$

where n_a stands for the number of coefficients actually computed and not degraded by image border effects.

It was shown in [25] that the anisotropy of the texture can be quantified by an index $\alpha \in [0, 2]$ ($\alpha = 1$ corresponding to isotropy) and that S_X often behaves as a power law, $S_X(j\hat{\alpha}_q, j(2-\hat{\alpha}_q), q) \simeq C2^{j\frac{q}{\hat{\alpha}_q}\hat{H}_q}$, where $\hat{\alpha}_q = \arg\max_\alpha \gamma(\alpha, q)$ is an estimate for α, $\hat{H}_q = -\gamma(\alpha, q)/q$ is an estimate for the (anisotropy robust) self-similarity, or Hurst, or fractal, parameter H, with $\gamma(\alpha, q) = \lim\inf_j \log_2(S_X(\alpha j, (2-\alpha)j, q))/j$. An example of $S_X(j_1, j_2, q = 2)$ is shown in Figure 4.

To ensure balanced contributions from all scales despite such power law behaviors, features are computed from $\log(S_X(j_1, j_2, q))$, after a normalization across scales that ensures that the features do not depend upon a change in the intensity of the raking light and exposure variables that influence overall image brightness

$$\tilde{S}_X(j_1, j_2, q) = \log(S_X(j_1, j_2, q)/\sum_{j_1', j_2'} S_X(j_1', j_2', q)). \quad (4)$$

In this article, the selected analysis scales are $1 \leq j_1, j_2 \leq 7$ and correspond to physical scales ranging from $13\,\mu m \leq a_1 = 2^{j_1}, a_2 = 2^{j_2} \leq 830\,\mu m \equiv 0.83$ mm (i.e., seven octaves) thus yielding a matrix of $7 \times 7 = 49$ multiscale features for texture characterization.

A cepstral-type distance (i.e., a log-transformed normalized L^p norm) between the multiscale representations $\tilde{S}_X(j_1, j_2, q)$ and $\tilde{S}_Y(j_1, j_2, q)$ is used to quantify proximity between textures X and Y defined as (with $p > 0$):

$$\mathcal{D}(X, Y) = \left(\sum_{j_1, j_2} |\tilde{S}_X(j_1, j_2, q) - \tilde{S}_Y(j_1, j_2, q)|^p\right)^{1/p}.$$

In this article, $q = 2$ and $p = 1$ are used, without specific tuning to obtain optimal results. The empirical distribution of the distances computed between all $(2491 \times 2490/2)$ pairs of samples in data set 2 is shown in Figure 5(a). The distances between some pairs among the samples in Figure 3 are superimposed to that distribution, and are also mapped into a

virtual 2-D space [cf. Figure 5(b)] quantifying resemblance and dissemblance between samples (mapping obtained by a standard multidimensional scaling procedure based on a Kruskal's normalized stress criterion).

Clustering is achieved via the spectral clustering procedure (cf., e.g., [26], [27], and [29]), which can be regarded as a specific unsupervised learning technique that aims to ensure robustness of the classification by reducing the dimensionality of the space in which samples are represented. Starting from the $N \times N$ cepstral distance matrix $\mathcal{D}$, where N is the number of photographic paper samples, the clustering procedure used here operates as follows.

1) A nonlinear transformation is applied to distance matrix $\mathcal{D}$, $\mathcal{A} = \exp(-\mathcal{D}/\epsilon)$ (corresponding here to entry-wise exponentiation), yielding a (dis)similarity matrix, where ϵ is a constant assessing the typical closeness between images.

2) The eigenvalues and eigenvectors of the (random walk-type) Laplacian operator $\mathcal{L} = I - D^{-1}\mathcal{A}$ associated to $\mathcal{A}$ are computed, where D is the diagonal matrix $D = \mathrm{diag}\left(\sum_j \mathcal{A}_{ij}\right)$.

3) The eigenvectors corresponding with the K smallest eigenvalues of $\mathcal{L}$ are assembled in the $K \times N$ matrix $\mathcal{S}$, defining the set of robust K coordinates (hence the reduction of dimensionality, $K \ll N$) for the N samples.

4) Hierarchical ascendant clustering (with Ward linkage) is applied to the matrix $\mathcal{S}$.

5) A set of thresholds is used to produce $K' \leq K$ hierarchical clusters.

RESULTS

DATA SET 1: TEST DATA SET

The analysis procedure described in the section "Methodology" yields the following results. Sorted eigenvalues of the Laplacian (and successive differences) as shown in the left plot of Figure 6(a) lead to conclude that $K = 13 \ll N = 120$ eigenvectors are sufficient to represent the distances within data set 1. The linkage procedure yields $K' = 7$ clusters that are robust to varying the linkage threshold, as shown on the dendrogram in Figure 6(b). The right plot of Figure 6(a) reports the intra- versus intercluster median distances, showing first the robustness of the achieved clustering (black diagonal squares indicate low intra-cluster median distance) and second the proximity of some clusters (e.g., 1 and 2 or 3 and 4). Inspection of the obtained clusters and comparison with the documentation available for data set 1 leads to the following striking conclusions:
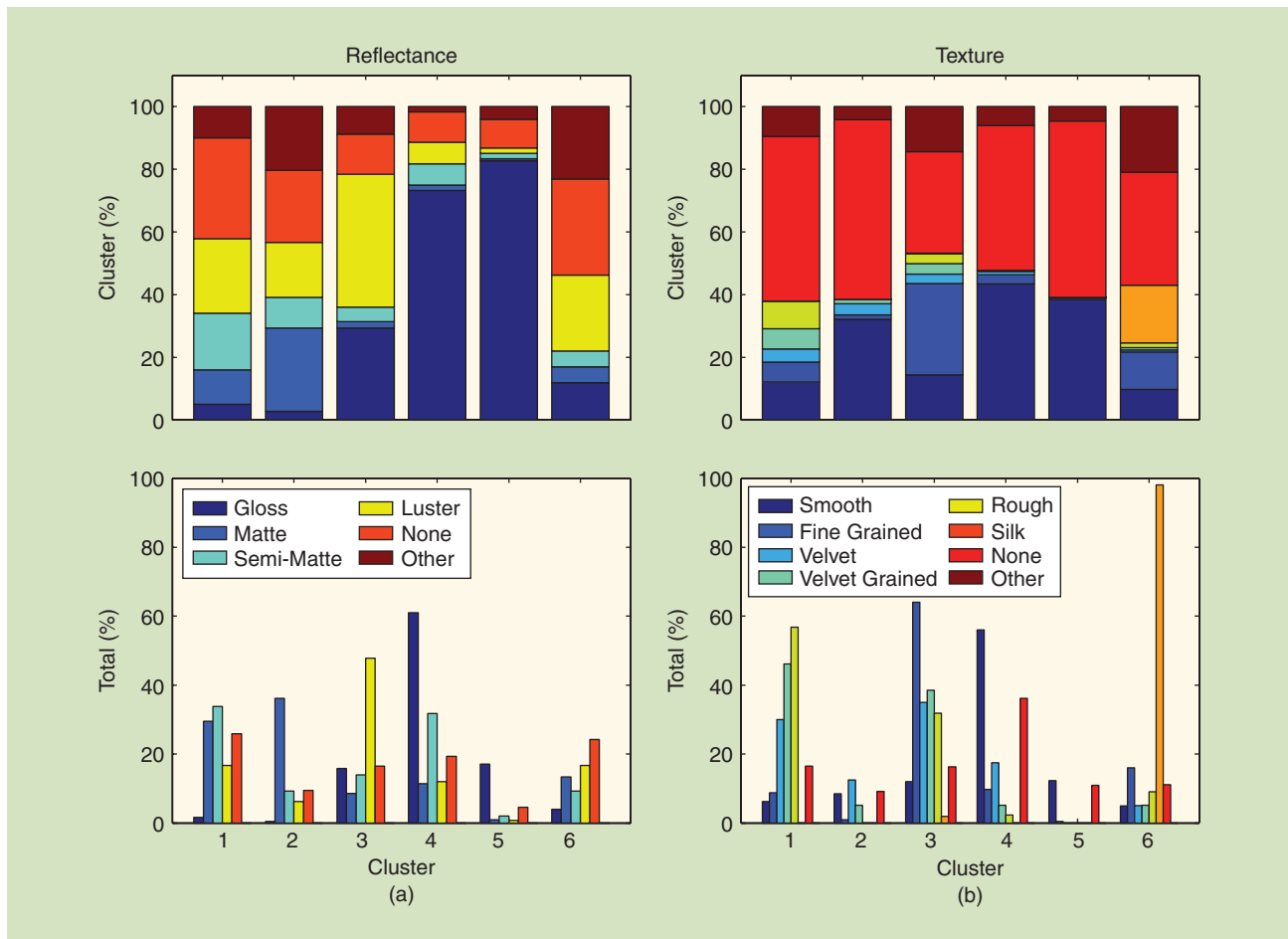
[FIG7] Data set 2: gross clustering. Achieved gross clusters are mostly driven first (a) by reflectance and second (b) by texture.

All ten samples from a same sheet—and, similarly, all ten samples from a same package—always fall in a common cluster. The median distances between the ten samples from the same sheet and the ten samples from different sheets of the same packet are found to be of the same order of magnitude, indicating a remarkable reproducibility of the manufacturing process [19], [20].

■ Samples from one given sheet or from one given packet correctly fall within the cluster containing different samples from the same manufacturer and produced to the same specifications of texture and reflectance.

■ From the semantic descriptions applied by the manufacturer, the attribute that mostly drives the clustering is reflectance, e.g., luster, chamois, matte, semimatte, and glossy. For the same reflectance (clusters 1 and 2, 3 and 4, and 6 and 7), the clustering is further refined by the manufacturer-applied terms describing texture, e.g., smooth, grained.

■ The classification of the 30 samples representing the diversity of photo papers is found to be clearly driven by both reflectance and texture.

The contents of $K' = 7$ clusters are summarized on the dendrogram in Figure 6(b) (see also [19] and [20]).

DATA SET 2: LARGE DATA SET

Application of the procedure described in the section "Methodology" to data set 2 leads to the following comments. Inspection of the sorted eigenvalues of the Laplacian and their successive differences shows that the use of $K = 62 \ll N = 2,491$ eigenvectors yields a robust representation of distances within data set 2.

GROSS CLUSTERING

Using classical tools to assess robustness and relevance in selecting the threshold of the linkage procedure applied in this $K = 62$ dimensional space leads to an initial coarse classification into $K' = 6$ large-size clusters $(143 \leq \text{Cluster Size} \leq 702)$. Compared to the semantic terms applied by manufacturers to describe gloss and texture, the analysis of these clusters leads to conclusions, reinforcing and enriching those drawn from the analysis of data set 1: clustering is mostly driven by reflectance and then texture, as illustrated in Figure 7. Clusters 4 and 5 correspond to a glossy reflectance, cluster 3 corresponds to a Luster reflectance, and clusters 1 and 2 correspond to matte and semimatte reflectances, with a rough or grained texture for the former and a velvet or smooth texture for the latter. Interestingly, cluster 6 gathers almost all of the unusually patterned

[FIG8] A cluster gathering of Willi Ruge's 1931 parachuting series. (Images courtesy of The Museum of Modern Art, New York).

silk textures (reflectance was not documented for most of these samples). See Figure 3 for representative examples of such reflectances and textures.

REFINED CLUSTERING

By decreasing the threshold of the linkage procedure, an increasing number of small-size clusters are extracted in a hierarchical manner, enabling a more detailed analysis of the data set. In some cases, these clusters have obvious interpretations for art scholars, including curators and conservators. For example, one of these clusters gathers 14 prints from a 1931 parachuting series by Willi Ruge (German, 1882–1961) from the Thomas Walther collection at the Museum of Modern Art (Figure 8). This series depicts groups of sequential exposures made to document several events. Grouping within a single cluster indicates the groups share a materials history and were likely made together. Other clusters suggest more surprising affinities and raise unexpected questions. Notably, a small cluster of three samples contains a platinum print by Alfred Stieglitz (American, 1864–1946) from 1915 and two palladium prints by Edward Weston (American, 1886–1958) from 1924 (Figure 9). Weston met the influential Stieglitz for the first time in 1922 during a short trip to New York. Weston said of this meeting [30, p. 5]: "Stieglitz has not changed my direction, only intensified it—and I am grateful." This small cluster possibly indicates that Stieglitz's influence was not simply a matter of artistic encouragement but perhaps also grounded in a deliberate use of the same materials. Given traditional modes of scholarships, the implied linkage between these prints would normally not receive scrutiny since these are different artists, using different imaging metals (platinum versus palladium), separated by a large geographical distance (California and New York) and a time period spanning nine years. However, clustering based on surface texture provokes new questions that might otherwise never be asked: Is the dating of the Stieglitz print secure (it is) or could it have been made later? Was Weston making a conscious effort to emulate Stieglitz even after the passage of nine years? Did manufacturers use essentially the same paper over long periods of time, even after the switch from platinum to palladium imaging metal after World War I? Are the overall warm image tones and especially the low contrast of the Stieglitz and the Weston cloud study attributes of a specific brand of paper? These and other related questions demonstrate how discovery of materials-based affinities can open the door to new modes of study.
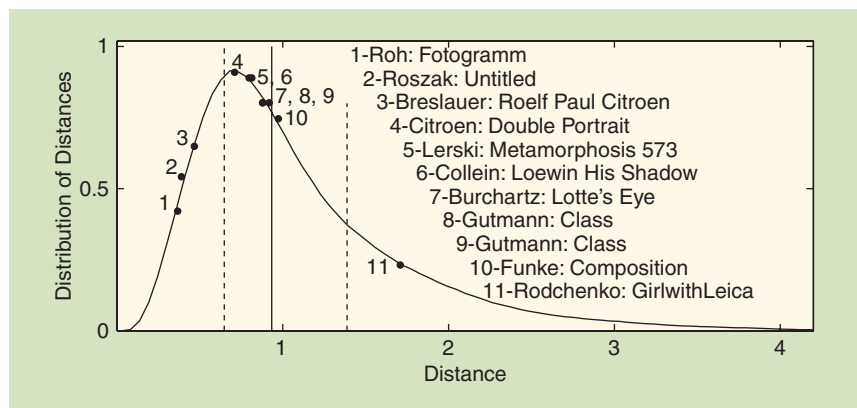
TWIN PRINTS

This promise is further illustrated by data set 2, where 11 pairs of prints, each pair attributed to the same artist and each showing the same or very similar image, are compared across two large museum collections, the Museum of Fine Arts, Houston, and the Museum of Modern Art in New York. The purpose of this comparison is to determine whether or not the pairs in the different collections are made on the same paper and thus have a shared materials-based history. For this comparison, four fundamental attributes can be compared, print thickness, highlight color, reflectance (or gloss), and texture, of which only the two last may have relations with the quantitative features used here to characterize photo paper surfaces. Figure 10 shows the overall empirical distribution of distances between all $(2491 \times 2490/2)$ pairs in data set 2 as a reference to compare the distances between the twin prints of the 11 pairs of interest here. For examples, the pairs by Franz Roh (German, 1890–1965), Theodore Roszak (American, 1907–1981), and Marianne Breslauer (German, 1909–2001) show small distances (corresponding respectively to the 5, 6,
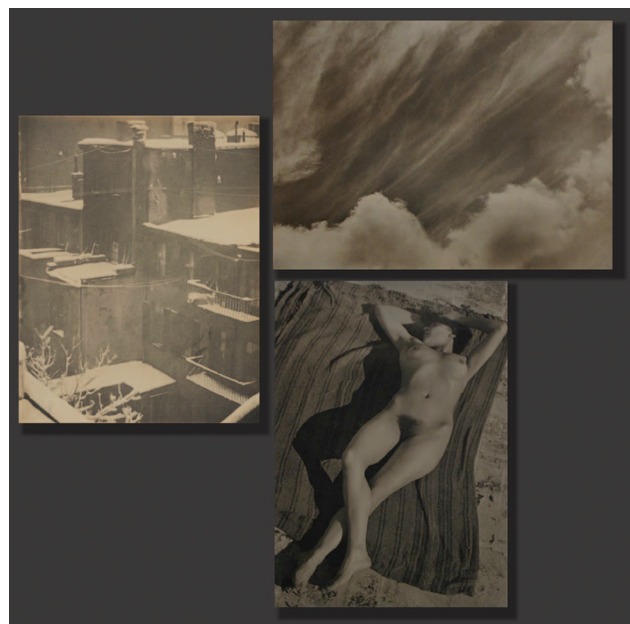
[FIG9] A surprising cluster gathering: one platinum print by A. Stieglitz from 1915 (left, © 2015 Georgia O'Keeffe Museum/Artists Rights Society, New York) and two palladium prints by E. Weston from 1924 (right) (images courtesy of The Museum of Modern Art, New York).

[FIG10] Distances between twin prints for the 11 pairs of interest, compared to the overall distribution of distances—the solid and dashed vertical lines denote, respectively, the 50% (or median distance) and 25% quantiles.

and 10% quantiles). Interestingly, the examination of print thickness, highlight color, reflectance, and texture had led to the conclusion that prints of these pairs were similar. For prints approaching a distance close to the distribution median distance (the solid vertical line in Figure 10), the similarities are less clear. In all respects (texture, reflectance, highlight color, and print thickness), pairs in this range by Max Burchartz (German, 1887–1961), John Gutmann (American, 1905–1998), and Jaromir Funke (Czech, 1896–1945) are classified as being on the same paper. However, pairs in this same range by Edmund Collein (German, 1906–1992), Helmar Lerski (Swiss, 1871–1956), and another Gutmann print are categorized as being on different paper when gloss, highlight color, and paper thickness are taken into account. In particular, the prints by Paul Citroen (Dutch, 1896–1983), though they have low texture differences (31% quantile), are classified as being on different paper mainly due to significant difference in gloss and print thickness. These results are not surprising given the common manufacturer practice of applying the same texture to different papers. These results suggest that an automated solution for discriminating material-based affinities across collections cannot rely on a single criterion, such as texture or reflectance, for determining results especially for distances around the median of the distribution.

Furthermore, such solutions should convey some level of confidence and context rather than returning a simple, binary determination of same or different. For distances significantly larger than the distribution median, the impact of color, thickness, and particularly gloss is still not clear. A pair by Alexander Rodchenko (Russian, 1891–1956) has a very large texture classification distance (beyond the 84% quantile) but could not be classified for this study due to missing information on gloss, highlight color, and print thickness. An interesting next step for prints such as those with large texture distances would be to determine whether additional information on, e.g., gloss or highlight color, have any impact on the determination of same or different or if instead the very large texture differences in this range are solely determinative.

CONCLUSIONS AND PERSPECTIVES

This article has quantitatively and qualitatively illustrated the potential value of basing the surface characterization and classification of photographic prints holding cultural value on anisotropic multiscale representations (HWT), combined with cepstral type distances and spectral clustering. The test data set 1 assembled in the framework of the Historic Photo Paper Classification Challenge demonstrates that the manufacturer-applied features of reflectance followed by texture are fundamental for the characterization of paper surfaces. Applied to data set 2, this methodology has promising results for art scholars, both by confirming existing conclusions and provoking new questions.

On the methodological side, this work can be expanded along several directions. There is an obvious need to compare the achieved results against those obtained with features both computed on other multiscale representations (e.g., [21]) or based on

representations of very different natures (cf. [19] for a first attempt). Devising distances that better match the perceptual, artistic, aesthetic and manufactured nature of photographic paper is a clear next step and an emergent priority. Also, at the clustering stages, tools for developing more robust assessments of both the relevance of a given cluster (compared to the benefit of further splitting it) as well as the confidence with which a given paper can be assigned to a given cluster, would significantly complement this first work. Additional strong benefits would likely result from using tools aiming at assessing the relevant levels at which data sets should be clustered, in the spirit of multiscale community clustering developed in, e.g., [29].

On the application side, texture characterization, comparison, classification, and retrieval systems have great potential within the humanities, promoting new modes of scholarship for curators, collectors, and art conservators. Dating, authentication, stylistic development, artistic intention, and spheres of artistic influence are vital scholarly questions. Networked and deployed across museum, library, and archive collections, methods for texture query and retrieval can lead to new research opportunities where a print in one location can be meaningfully compared, based on physical attributes, to others held elsewhere. Such systems will provide the means to discover material-based (not simply image-based) affinities across time and within and across artists' oeuvres. Intrinsically valuable for enhanced scholarship in the humanities, such systems also would be effective for identifying anomalies, notably including fakes.

A key future step lies in further developing tools permitting deeper and more meaningful interactions between signal and image processing experts and scholars working within a wide array of humanities-based disciplines. Besides simply making lists of clusters available to humanities-based experts, such tools must enable them to naturally apprehend the robustness of proposed clustering (or its fragility), its hierarchical nature as well as its sensitivity to methodological choices. Developed further, such systems would optimally allow for qualitative input and the modeling of results based on other bodies of nonempirical knowledge. This work would present exciting opportunities where the fields of signal and image processing can adapt to the subtleties and specificities of humanities disciplines, thus broadening applications and cross-disciplinary relevance.

AUTHORS

Patrice Abry (patrice.abry@ens-lyon.fr) is a senior researcher with the CNRS at Ecole Normale Supérieure de Lyon, France. He is developing a long-standing research program on the theoretical modeling and analysis of scale invariance and applications.

Stéphane G. Roux (stephane.roux@ens-lyon.fr) is an assistant professor at Ecole Normale Supérieure de Lyon, France, where he is a specialist in wavelet analysis and their practical application in physics, geophysics, and biology.

Herwig Wendt (herwig.wendt@irit.fr) is an associate researcher with the CNRS. His main focus is on scale invariance and multifractal analysis, particularly for images, and statistical estimation.

Paul Messier (pm@paulmessier.com) is the head of the Lens Media Lab, Yale University, New Haven, Connecticut, and consults internationally with individual collectors and institutions.

Andrew G. Klein (andy.klein@wwu.edu) is an assistant professor of engineering and design at Western Washington University, where he studies signal processing and distributed communication systems.

Nicolas Tremblay (nicolas.tremblay@ens-lyon.fr) is a Ph.D. student at Ecole Normale Supérieure de Lyon, France, and is interested in signal processing over networks and network-based classification techniques.

Pierre Borgnat (pierre.borgnat@ens-lyon.fr) is an associate researcher with CNRS at Ecole Normale Supérieure de Lyon, France, and is working on nonstationary and multiscale signal processing as well as graph signal processing, developing applications for complex systems and networks.

Stéphane Jaffard (stephane.jaffard@u-pec.fr) is a professor of mathematics at Université Paris-Est Creteil, France. He is working on wavelet and multifractal analysis. He is a former president of the French Mathematical Society.

Béatrice Vedel (beatrice.vedel@univ-ubs.fr) is an associate professor of applied mathematics at Université de Bretagne Sud, France. She is working on multifractal analysis, wavelets analysis, and function spaces theory.

Jim Coddington (jim_coddington@moma.org) is the chief conservator of the Museum of Modern Art in New York. He has published articles on imaging, structural restoration, and studies of modern painters.

Lee Ann Daffner (leeann_daffner@moma.org) is the Andrew W. Mellon Conservator of Photographs and is responsible for the preservation, conservation, and research initiatives of the Museum of Modern Art's photography collection.

REFERENCES

[1] P. Messier. (2013). The Paul Messier black and white photographic papers collection. [Online]. Available: http://paulmessier.com/pm/pdf/papers/historic_photographic_papers_collection.pdf

[2] P. Messier, C. R. Johnson, H. Wilhelm, W. A. Sethares, A. G. Klein, P. Abry, S. Jaffard, H. Wendt, S. G. Roux, N. Pustelnik, N. van Noord, L. van der Maaten, and E. Postma, "Automated surface texture classification of inkjet and photographic media," in *Proc. Int. Conf. Digital Printing Technologies*, Seattle, WA, 2013, pp. 85–91.

[3] P. Messier, "Photographic papers in the 20th century: Methodologies for research, authentication and dating," in *Proc. FotoConservación*, Logroño, Spain, 2011.

[4] R. M. Haralick, "Statistical and structural approaches to texture," *Proc. IEEE*, vol. 67, no. 5, pp. 786–804, 1979.

[5] M. M. Galloway, "Texture analysis using gray level run lengths," *Comput. Vision Graph.*, vol. 4, no. 2, pp. 172–179, 1975.

[6] K. Deguchi, "Two-dimensional auto-regressive model for analysis and synthesis of gray-level textures," in *Proc. Int. Symp. Science on Form*, 1986, pp. 441–449.

[7] Y. Stitou, F. Turcu, Y. Berthoumieu, and M. Najim, "Three-dimensional textured image blocks model based on Wold decomposition," *IEEE Trans. Signal Processing*, vol. 55, no. 7, pp. 3247–3261, July 2007.

[8] A. M. Atto, Y. Berthoumieu, and P. Bolon, "2-dimensional wavelet packet spectrum for texture analysis," *IEEE Trans. Image Processing*, vol. 22, no. 22, pp. 2495–2500, June 2013.

[9] P. Kestener, J. Lina, P. Saint-Jean, and A. Arneodo, "Wavelet-based multifractal formalism to assist in diagnosis in digitized mammograms," *Image Anal. Stereol.*, vol. 20, no. 3, pp. 169–175, 2004.

[10] R. Lopes and N. Betrouni, "Fractal and multifractal analysis: A review," *Med. Image Anal.*, vol. 13, no. 4, pp. 634–649, 2009.

[11] N. Mallick, P. P. Cortet, S. Santucci, S. G. Roux, and L. Vanel, "Discrepancy between subcritical and fast rupture roughness: A cumulant analysis," *Phys. Rev. Lett.*, vol. 98, p. 255502, 2007.

[12] S. G. Roux, A. Arneodo, and N. Decoster, "A wavelet-based method for multifractal image analysis. III. Applications to high-resolution satellite images of cloud structure," *Eur. Phys. J. B*, vol. 15, no. 4, pp. 765–786, 2000.

[13] P. Abry, J. Coddington, I. Daubechies, E. Hendriks, S. Hughes, R. Johnson, and E. Postma., "Special issue on image processing for digital art work guest editor's forewords," *Signal Process*. (special issue), vol. 93, pp. 525–526, 2013.

[14] M. Barni, J.-A. Beraldin, C. Lahanier, and A. Piva., "Signal processing in visual cultural heritage," *IEEE Signal Process. Mag.*, vol. 25, no. 4, pp. 10–13, 2008.

[15] C. Benhamou, S. Poupon, E. Lespessailles, S. Loiseau, R. Jennane, V. Siroux, W. J. Ohley, and L. Pothuaud, "Fractal analysis of radiographic trabecular bone texture and bone mineral density: two complementary parameters related to osteoporotic fractures," *J. Bone Miner. Res.*, vol. 16, no. 4, pp. 697–704, 2001.

[16] D. Rockmore, J. Coddington, J. Elton, and Y. Wang, "Multifractal analysis for Jackson Pollock," *Proc. SPIE*, pp. 6810–6813, 2008.

[17] P. Abry, H. Wendt, and S. Jaffard, "When Van Gogh meets Mandelbrot: Multifractal classification of painting's texture," *Signal Process*. (special issue), vol. 93, no. 3, pp. 554–572, 2013.

[18] P. Abry, S. Jaffard, and H. Wendt, "Bruegel's drawings under the multifractal microscope," in *Proc. IEEE Int. Conf. Acoustics, Speech, Signal Processing (ICASSP)*, Kyoto, Japan, 2012, pp. 3909–3912.

[19] C. R. Johnson, P. Messier, W. A. Sethares, A. G. Klein, C. Brown, P. Klausmeyer, P. Abry, S. Jaffard, H. Wendt, S. G. Roux, N. Pustelnik, N. van Noord, L. van der Maaten, E. Postma, J. Coddington, L. A. Daffner, H. Murata, H. Wilhelm, S. Wod, and M. Messier, "Pursuing automated classification of historic photographic papers from raking light photomicrographs," *J. Amer. Inst. Conserv.*, vol. 53, no. 3, pp. 159–170, 2014.

[20] P. Abry, S. Roux, H. Wendt, and S. Jaffard, "Hyperbolic wavelet transform for photographic paper texture characterization," in *Proc. Asilomar Conf. Signals, Systems, Computers*, Nov. 2014.

[21] A. G. Klein, A. Do, C. A. Brown, and P. Klausmeyer, "Classification via area-scale analysis of raking light images," in *Proc. Asilomar Conf. Signals, Systems, Computers*, Nov. 2014.

[22] W. A. Sethares, A. Ingle, T. Krc, and S. Wood, "Eigentextures: An SVD approach to automated paper classification," in *Proc. Asilomar Conf. Signals, Systems, Computers*, Nov. 2014.

[23] H. Wendt, S. G. Roux, P. Abry, and S. Jaffard, "Wavelet leaders and bootstrap for multifractal analysis of images," *Signal Process.*, vol. 89, pp. 1100–1114, 2009.

[24] R. A. DeVore, S. V. Konyagin, and V. N. Temlyakov, "Hyperbolic wavelet approximation," *Construct. Approx.*, vol. 14, no. 1, pp. 1–26, 1998.

[25] S. G. Roux, M. Clausel, B. Vedel, S. Jaffard, and P. Abry, "Self-similar anisotropic texture analysis: The hyperbolic wavelet transform contribution," *IEEE Trans. Image Processing*, vol. 22, no. 11, pp. 4353–4363, 2013.

[26] U. Von Luxburg, "A tutorial on spectral clustering," *Stat. Comput.*, vol. 17, no. 4, pp. 395–416, 2007.

[27] T. Hastie, R. Tibshirani, and J. Friedman, *The Elements of Statistical Learning* (Springer Series in Statistics). New York: Springer, 2001.

[28] S. Mallat, *A Wavelet Tour of Signal Processing*. San Diego, CA: Academic Press, 1998.

[29] N. Tremblay and P. Borgnat, "Graph wavelets for multiscale community mining," *IEEE Trans. Signal Processing*, vol. 62, no. 20, pp. 5227–5239, 2014.

[30] E. Weston, *The Daybooks of Edward Weston*, N. Newhall, Ed. New York: Aperture, 1973.

[SP]